Crystal Structures of Aged Phosphonylated Acetylcholinesterase: Nerve Agent Reaction Products at the Atomic Level[†,‡]

Charles B. Millard,*[,§] Gitay Kryger,[||] Arie Ordentlich,[⊥] Harry M. Greenblatt,[||] Michal Harel,[||] Mia L. Raves,[||,#] Yoffi Segall,[⊥] Dov Barak,[⊥] Avigdor Shafferman,[⊥] Israel Silman,[▽] and Joel L. Sussman[||,⊗]

Departments of Neurobiology and Structural Biology, Weizmann Institute of Science, Rehovot 76100, Israel, and Israel Institute for Biological Research, Ness Ziona 70450, Israel

Received November 10, 1998; Revised Manuscript Received March 26, 1999

ABSTRACT: Organophosphorus acid anhydride (OP) nerve agents are potent inhibitors which rapidly phosphonylate acetylcholinesterase (AChE) and then may undergo an internal dealkylation reaction (called "aging") to produce an OP-enzyme conjugate that cannot be reactivated. To understand the basis for irreversible inhibition, we solved the structures of aged conjugates obtained by reaction of *Torpedo californica* AChE (*Tc*AChE) with di*iso*propylphosphorofluoridate (DFP), *O*-*iso*propylmethylphosphonofluoridate (sarin), or *O*-pinacolylmethylphosphonofluoridate (soman) by X-ray crystallography to 2.3, 2.6, or 2.2 Å resolution, respectively. The highest positive difference density peak corresponded to the OP phosphorus and was located within covalent bonding distance of the active-site serine (S200) in each structure. The OP-oxygen atoms were within hydrogen-bonding distance of four potential donors from catalytic subsites of the enzyme, suggesting that electrostatic forces significantly stabilize the aged enzyme. The active sites of aged sarin- and soman-*Tc*AChE were essentially identical and provided structural models for the negatively charged, tetrahedral intermediate that occurs during deacylation with the natural substrate, acetylcholine. Phosphorylation with DFP caused an unexpected movement in the main chain of a loop that includes residues F288 and F290 of the *Tc*AChE acyl pocket. This is the first major conformational change reported in the active site of any AChE−ligand complex, and it offers a structural explanation for the substrate selectivity of AChE.

Acetylcholinesterase (AChE[1]) is an especially efficient serine hydrolase that catalyzes the breakdown of acetylcholine (ACh) at cholinergic synapses (reviewed in ref *1*). The reaction of AChE with carboxyl ester substrates, including ACh, is believed to proceed through an unstable tetrahedral intermediate (TI) before collapsing to a short-lived ($t_{1/2}$ ∼50 μs) acetyl-enzyme (*2*) (Scheme 1). The acetyl-enzyme subsequently undergoes nucleophilic attack by water, passing through a second TI, and the regenerated enzyme is expelled as the leaving group (deacylation). The two-step catalytic

Scheme 1: Reaction of AChE with a Natural Carboxyl Ester Substrate, Such as ACh[a]

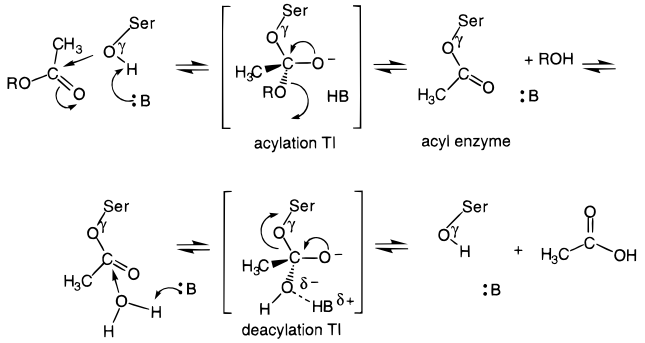

[a] The scheme begins with the reversible enzyme−substrate complex and ends with free enzyme. The enzyme's catalytic general base, probably Nϵ2 of His440, is depicted as :B, and the first product is depicted as ROH (choline in the case of ACh). The top panel shows acylation and the lower panel shows deacylation. For both reactions, the carbonyl carbon is expected to proceed from its planar geometry to a tetrahedral intermediate with an asymmetric negative charge distribution (depicted in brackets) during nucleophilic attack. Note that the theoretical deacylation TI for AChE is expected to resemble the aged OP-AChE conjugate (depicted in Scheme 2).

[†] The U.S. Army Medical Research & Materiel Command (agreements DAMD17-97-2-7022 and DAMD17-96-C-6088) and the U. S. Army Scientist/ Engineer Exchange Program supported this project. The work was presented in preliminary form at the sixth International Meeting on Cholinesterases & Related Proteins, La Jolla, CA, 1998, and at the U.S. Army Bioscience Review, Hunt Valley, MD, 1998.

[‡] Coordinates for the solved crystal structures have been deposited in the Brookhaven Protein Data Bank, Biology Department, Brookhaven National Laboratory, Upton, NY 11973 under accession codes 1som (soman), 1cfj (sarin), and 2dfp (DFP).

* Corresponding author e-mail: limill@sgjs6.weizmann.ac.il.

[§] Visiting scientist at the Weizmann Institute from the U.S. Army Medical Research Institute of Chemical Defense, APG, MD 21010-5425.

[||] Department of Structural Biology, The Weizmann Institute of Science.

[⊥] Israel Institute for Biological Research.

[#] Present address: Department of NMR Spectroscopy, Bijvoet Center for Biomolecular Research, Utrecht University, 3584 CH Utrecht, The Netherlands.

[▽] Department of Neurobiology, The Weizmann Institute of Science.

[⊗] Biology Department, Brookhaven National Laboratory, Upton, NY 11973.

[1] Abbreviations: ACh, acetylcholine; AChE, acetylcholinesterase (EC 3.1.1.7); ATCh, acetylthiocholine; BChE, butyrylcholinesterase (EC 3.1.1.8); BTCh, butyrylthiocholine; DFP, diisopropylphosphorofluoridate; Hu, human; MeP-, methylphosphonylated; MES, (2-[*N*-morpholino]ethanesulfonic acid); M*i*PrP-, mono*iso*propylphosphorylated; OP, organophosphorus acid anhydride; PDB, Protein Data Bank; PEG, poly(ethylene glycol); rmsd, root-mean-square deviation; *Tc*, *Torpedo californica*; TI, tetrahedral intermediate; TMTFA, *m*-(*N*,*N*,*N*-trimethylammonio)-2,2,2-trifluoroacetophenone.

10.1021/bi982678l CCC: $18.00
Published on Web 05/11/1999

Scheme 2: Reaction of AChE with a Phosphonate Nerve Agent[a]

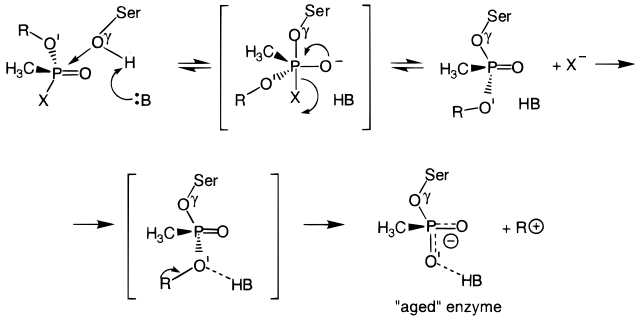

[a] The scheme begins with the reversible enzyme-OP complex and ends with irreversibly inhibited aged enzyme. The phosphylation leaving group is depicted as X (fluoride ion in the case of soman, sarin, or DFP); the enzyme's catalytic general base, probably Nϵ2 of His440, is depicted as :B; R is a branched alkyl group; and R+ is a hypothetical carbonium ion which reacts in water to yield primarily the alcohol product, ROH (9). The top panel shows phosphylation, and the lower panel shows dealkylation (aging). Phosphonylation is expected to occur via a trigonal bipyramidal intermediate (depicted in brackets in the upper panel), or a transition state resembling such a structure, with inversion of stereochemistry at P. For reaction of AChE with DFP, an -O*i*Pr group replaces the -CH_3 bonded to P.

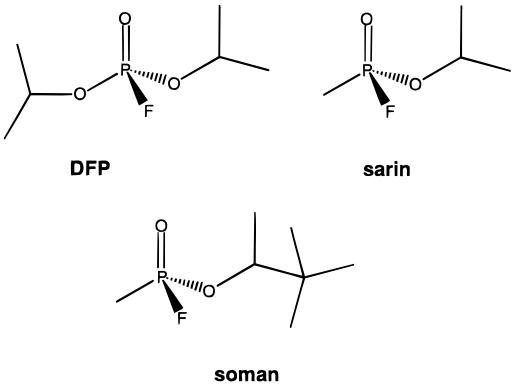

FIGURE 1: Chemical formulas of the OP inhibitors (non-hydrogen atoms).

mechanism renders AChE susceptible to rapid, stoichiometric, and essentially irreversible inhibition by a class of organophosphorus acid anhydride (OP) inhibitors, typified by di*iso*propylphosphorofluoridate (DFP) and the phosphonate nerve agents, which can act as "hemisubstrates" to trap the enzyme in a structure that closely resembles the negatively charged deacylation TI (*3*) (Scheme 2).

Unlike the intermediates formed with carboxyl esters, the OP-enzyme persists for many hours or days (reviewed in ref *4*). Slow hydrolysis has been explained by steric exclusion; the active-site histidine (H440) is not positioned to carry a water molecule to the correct face of the phosphorus required for nucleophilic attack (*5*, *6*). It also has been proposed that H440 is rendered ineffective as a general base because the imidazolium forms an unproductive hydrogen bond with an oxygen atom of the OP (*7*).

After phosphylation[2] of the active-site serine, some OP-AChE conjugates undergo post-inhibitory reactions, collectively called "aging", which result in truly irreversible enzyme inhibition (Scheme 2). The best-characterized aging reaction is that of AChE inhibited by DFP, *O-iso*propylmethylphosponofluoridate (sarin), or *O*-pinacolylmethylphosphonofluoridate (soman). These inhibitors possess a branched alkyl group (Figure 1) which has been proposed to undergo dealkylation by a carbonium ion mechanism, thereby adding a formal negative charge to the active site of phosphylated AChE (*8*, *9*).

The X-ray crystallographic structure of *Torpedo californica* (Tc) AChE (*10*) and computer-based homology models of human (Hu) AChE (*11*) and the closely related serum enzyme butyrylcholinesterase (BChE; refs *12*, *13*), combined with site-directed mutagenesis studies, have permitted tentative identification of the specific amino acid residues which constitute several catalytic subsites, including an "oxyanion hole" (*14*), a hydrophobic acyl pocket, and a trimethylammonium (choline) binding site (reviewed in ref *15*). Direct demonstration of these subsites with natural substrates has not been achieved because of the inherent instability of the intermediates that form during carboxyl ester hydrolysis. Our goal was to solve the three-dimensional structures of aged phosphylated *Tc*AChE as a means of (1) understanding the forces that oppose reactivation (dephosphylation) of the OP-enzyme, and (2) providing structural models for the deacylation TI of carboxyl ester hydrolysis which could validate the topography of the AChE active site.

MATERIALS AND METHODS

*Enzyme Purification and Characterization. Tc*AChE was purified as described (*16*), and the steady-state constants for its reactions with acetylthiocholine (ATCh), butyrylthiocholine (BTCh), and DFP were measured using previously described methods (*17*, *18*). Briefly, the catalytic activity was determined for substrates ATCh and BTCh by the spectrophotometric method of Ellman (*19*). Substrate Michaelis constants (K_m) and catalytic rate constants (k_{cat}) were derived from Lineweaver−Burk plots and from direct nonlinear curve fitting of the rate equation. The steady-state dissociation constant (K_d) and phosphorylation rate constant (k_2) for the reaction of DFP with *Tc*AChE were measured by monitoring continuous inhibition curves in the presence of excess substrate (ATCh) (*18*, *20*). All kinetic experiments were done in 50 mM phosphate buffer, pH 8.0, 24 °C.

Crystallization of OP-TcAChE Conjugates. Purified *Tc*AChE was inhibited with DFP, sarin, or soman.[3] DFP and sarin were used at 300-fold molar excess to enzyme, and soman was used at 2100-fold molar excess. The aging reaction proceeded to >95% completion; aliquots of the OP-*Tc*AChE conjugates could not be reactivated by 20 h incubation with either 10 mM pyridine-2-aldoxime methiodide or 1,1′-trimethylene-bis(4-formylpyridinium bromide) dioxime. Unbound OP was removed by gel filtration before the crystallization experiments.

OP-*Tc*AChE conjugates were crystallized in hanging drops by the vapor diffusion method. Protein crystallized at a concentration of 10 mg/mL from a precipitating solution of 35−40% w/v PEG-200 (Sigma Chemicals, St. Louis, MO) in 0.15 M MES buffer, 0.05 M NaCl, pH 5.8−6.0 at 4 °C.

[2] The term "phosphylated" denotes phosphorylation and phosphonylation reactions without distinction.

[3] The OP inhibitors are extremely toxic; sarin and soman were handled according to established regulations governing chemical warfare materials.

Table 1: Kinetic Constants for Reaction of ATCh, BTCh, or DFP with *Tc*AChE, HuAChE, or HuBChE[a]

	substrate hydrolysis (k_{cat}/K_m) × 10^{-8} (M^{-1} min^{-1})		DFP inhibition		
	ATCh	BTCh	k_i × 10^{-4} ($M^{-1}min^{-1}$)	k_2 (min^{-1})	K_d (μM)
*Tc*AChE	46 ± 5	0.10 ± 0.01	2.0 ± 0.1	1.5 ± 0.5	70 ± 20
HuAChE[b]	30 ± 4	0.30 ± 0.05	5.0 ± 0.1	0.6 ± 0.1	13 ± 2
HuAChE F295L/F297V[c]	2.2 ± 0.3	14 ± 3	800 ± 60	0.8 ± 0.1	0.10 + 0.02
HuBChE[d]	3.4 ± 0.5	7 ± 1	1660 ± 50	1.0 ± 0.2	0.06 ± 0.01

[a] Each value is the mean ± standard error of at least four repetitions. [b] Recombinant, wild-type HuAChE expressed in 293 embryonic kidney cells (*17*, *18*). [c] HuAChE mutant in which the acyl pocket residues corresponding to F288 and F290 in *Tc*AChE have been replaced with those found in the sequence of HuBChE (*17*, *18*). [d] Recombinant wild-type HuBChE expressed in 293 cells.

Although suitable crystals appeared spontaneously after 5−10 days, their quality was improved by seeding with microscopic crystalline fragments.

X-ray Diffraction and Data Processing. The exterior mother liquor that surrounds the crystals during their growth was exchanged with high-viscosity motor oil (Exxon, Houston, TX), and the crystals subsequently were flash-cooled in liquid nitrogen (*21*). X-ray diffraction data were collected at 100 K. Data for the DFP and soman conjugates were collected at the Weizmann Institute of Science using a Rigaku rotating anode FR300 (50 mA, 50 kV) source (λ = 1.54 Å) with a Rigaku Raxis-II detector. For the sarin conjugate, data were collected using the U.S. National Synchrotron Light Source at Brookhaven National Laboratory on beamline X12C (λ = 1.1 Å), with a 2 × 2 Brandeis charge-coupled device detector. Data collection parameters were optimized using the computer program STRATEGY (*22*), and intensity data were processed with DENZO and SCALEPACK (*23*).

Model Refinement. The 2.5 Å structure of native *Tc*AChE (2ace in the Brookhaven Protein Data Bank, PDB) (*24*) was used to obtain the initial models by rigid-body refinement and simulated annealing (*25*). The solvent, carbohydrate, and OP atoms subsequently were built into ($F_o - F_c$) electron density difference maps. All three structures were refined by a combination of simulated annealing and torsion angle molecular dynamics with a maximum likelihood target function, using the programs of Crystallography & NMR System, CNS v.0.5 (*26*, *27*). The quality of the refined structures was assessed using PROCHECK (*28*) and WHATIF (*29*). The Cα atom positions of the OP-*Tc*AChE structures were compared with those of native *Tc*AChE using PROFIT (SciTech Software, University College, London). The program INSIGHTII v.97.0 (Biosym Technologies, San Diego, CA) was used to calculate the positions of hydrogen atoms, to generate theoretical solvent-accessible surfaces, and to produce the final figures.

RESULTS

Reaction Kinetics. The reaction rate constants of *Tc*AChE with ATCh, BTCh, or DFP were similar to those of HuAChE, but considerably different from those of HuBChE (Table 1). For example, the K_d for the reversible complex of *Tc*AChE and DFP was 6-fold less than that measured for HuAChE using identical methodology (*18*), but it was over 1200-fold less than that measured for HuBChE (Table 1).

X-ray Crystallography. Data were collected from trigonal crystals of space group $P3_121$ (*10*) and refined to 2.3 (DFP), 2.6 (sarin), or 2.2 Å (soman) resolution (Table 2). The highest positive difference density peak (>15σ) in the initial ($F_o - F_c$) maps corresponded to the phosphorus of the OP and was observed to be within covalent bonding distance of the S200 Oγ in all three structures (Figure 2). Only one peak of this magnitude was found in each structure; this result confirmed that OP nerve agents form a covalent bond exclusively with the active-site serine of AChE (*30*).

Table 2: Crystallographic Data Collection and Refinement Statistics

	M*i*PrP-AChE (DFP)	MeP-AChE (sarin)	MeP-AChE (soman)
Data Collection			
resolution (Å)	20−2.3	30−2.6	30−2.2
total number of reflections	278 106	200 755	286 328
unique reflections	42 410	30 011	49 048
% completeness: overall (highest refinement shell)	94.2 (66.3)	97.4 (99.3)	96.7 (94.1)
R_{sym}[a]: overall (highest refinement shell)	0.07 (0.41)	0.09 (0.17)	0.05 (0.30)
average *I*/average σ: overall (highest refinement shell)	15.9 (1.7)	10.3 (2.2)	15.6 (2.6)
Refinement			
R factor[b] (no σ cutoff) (%)	18.6	18.6	21.0
number of reflections in working set	40 334	27 034	46 332
R free[c] (no σ cutoff) (%)	22.7	24.7	25.1
number of reflections in test set (% total)	1874 (4.2)	1497 (4.9)	2460 (4.9)
rmsd bond lengths (Å)	0.02	0.02	0.02
rmsd bond angles (deg)	1.9	2.0	1.9
total number of nonhydrogen atoms	4729	4497	4390
protein	4263	4245	4174
carbohydrate	70	28	28
inhibitor	7	4	4
water (MES[d])	377 (12)	220	184

[a] $R_{sym} = \sum|I - \langle I\rangle|/\sum I$, where *I* is an individual reflection measurement and $\langle I\rangle$ is the mean intensity for symmetry-related reflections. [b] R-factor = $\sum||F_o| - |F_c||/\sum|F_o|$, where F_o and F_c are observed and calculated structure factors, respectively. [c] *R* free is calculated for randomly selected reflections excluded from refinement. [d] A single molecule of MES (crystallization buffer) was refined on the surface of the M*i*PrP-AChE structure, adjacent to the *Tc*AChE carboxyl-terminal α-helix. The MES molecule was apparently stabilized by the side-chain nitrogen atoms of Q500 and N409, as well as by a water molecule within possible hydrogen-bond distance to the imidazole ring of H406 (not shown).

The overall orientation of the bound OP, relative to the active-site gorge, was comparable in all three structures (Figures 3 and 4). There were no detectable alterations in the geometry of the active-site triad (S200-H440-E327) of the aged OP-*Tc*AChE structures, compared with that of native *Tc*AChE. A water molecule that is normally present within hydrogen-bond distance of the oxyanion hole in the active site of native *Tc*AChE (water no. 682 in 2ace) was displaced by the OP in each structure.

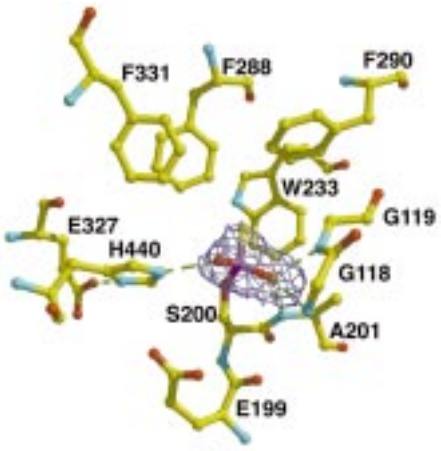

FIGURE 2: Initial difference electron density map for MeP-AChE. The final, refined active site of aged MeP-AChE, obtained by reaction with soman, is superimposed on the initial ($F_o - F_c$) electron density map (30−2.2 Å all data; map contour level 3σ) after rigid-body refinement of the protein, but before including the OP moiety in the refinement. Only density that is within 2.0 Å of the soman atoms is contoured. Note that the tetrahedral geometry of the soman phosphorus atom was clearly apparent in the initial, unbiased difference maps.

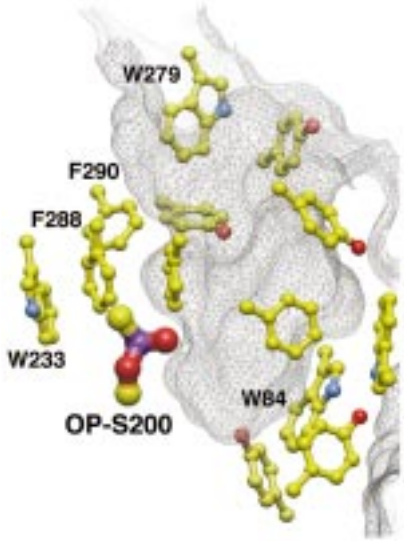

FIGURE 3: Orientation of the bound OP relative to the active-site gorge. The structure depicted is that of aged MeP-*Tc*AChE (soman) viewed down the P═O bond with the oxyanion hole oxygen atom (not visible) directly behind the phosphorus atom (colored purple). The position of the phosphonylated serine (OP-S200) is shown relative to those of the thirteen aromatic side chains that line the active-site gorge of AChE (*10*). The solvent-accessible surface (spherical probe of 1.4 Å radius) was calculated for 16 Å around the OP (grey mesh). Note that the OP methyl group is buried in a hydrophobic patch formed by W233, F288, and F290, but the oxygen that undergoes dealkylation (O′ Scheme 2) points toward a solvent-accessible pocket in front of W84.

The strong stereoselectivity of AChE ensured that, under our experimental conditions, the primary OP reactants were the P_S stereoisomers of sarin and soman (*31*). The MeP-AChE structures establish the stereochemistry of the final reaction products and, thereby, demonstrate an overall inversion of the absolute configuration at the OP phosphorus (Figure 4). Inversion is consistent with a simple in-line nucleophilic attack by the S200 Oγ during phosphylation (Scheme 2), but the structures do not exclude more complicated reaction mechanisms.

At completion of the post-inhibitory aging process, the final reaction product was an anionic methylphosphonylated (MeP)-AChE in the case of sarin and soman, or an anionic monoisopropylphosphorylated (M*i*PrP)-AChE with DFP (Figure 4). Direct observation of the dealkylated OPs after aging proves that the original interpretations of low-molecular-mass product analysis (*8*, *9*) and recent mass spectrometric data (*32*) were fundamentally correct.

In all three aged OP-*Tc*AChE structures, the oxygen atom of the OP that underwent dealkylation (designated O′ in Scheme 2) was oriented toward a polar pocket in the active site that contained several water molecules (corresponding to waters no. 633, 678, 679, and 742 in 2ace). At least one of these waters (no. 742 in 2ace) must move to accommodate the alkyl group that departs during aging. The geometry between O′ and H440 Nϵ2 was consistent with the presence of an imidazolium at H440 that could act as a hydrogen-bond donor (Table 3).

The overall root-mean-square deviation (rmsd) for Cα atoms, relative to native *Tc*AChE, was only 0.3 Å for each MeP-AChE structure and 0.4 Å for M*i*PrP-AChE. There was an unexpected conformational change, however, in the active-site acyl pocket of the M*i*PrP-AChE structure. The side chains of F288 and F290 moved significantly, and the main chain underwent "peptide flips" (*33*) between I287 and S291 to accommodate one of the *iso*propyl groups of DFP (Figures 4C and 5). The ψ-dihedral angle for I287 changed by 184°, moving from $\psi = 140°$ in native *Tc*AChE to $\psi = -44°$ in M*i*PrP-AChE. This flip in the I287 ψ-dihedral angle was offset by successive changes in the ψ-dihedral angles for R289, F290, and S291. The calculated deviation for the Cα atoms in residues 287−291 in the M*i*PrP-AChE structure, compared with native *Tc*AChE, was 0.6, 2.9, 4.8, 2.2, and 0.8 Å, respectively.

A more subtle repositioning of F331 by rotation around its χ1 and χ2 angles also occurred in the M*i*PrP-AChE acyl pocket (not shown). The phenyl ring of F331 moved and partially filled the space created by displacement of the phenyl ring of F288.

The conformational change in M*i*PrP-AChE did not appear to be a consequence of the dealkylation reaction (aging), because no evidence was found for a significant conformational change in the other two aged structures. Moreover, the residues in the acyl pocket of the sarin conjugate showed no detectable movement, despite the fact that both DFP and sarin lose an identical *iso*propyl group during the dealkylation reaction (Scheme 2).

DISCUSSION

Serine hydrolases may catalyze the phosphylation and aging reactions with OP inhibitors containing branched alkyl groups, and thus greatly accelerate their own irreversible inhibition (*7*, *34*). The remarkably large rate enhancement of the aging reaction by cholinesterase has been ascribed to the precise juxtaposition of the departing alkyl group with specific amino acid residues in the enzyme active site (*35*−*37*).

The aged OP-*Tc*AChE structures do not permit direct observation of the alkyl group that departs during dealkylation, but its general topography on the enzyme surface can be deduced from the steric constraints of the phosphylated active site (*38*). On the basis of the position of the residual

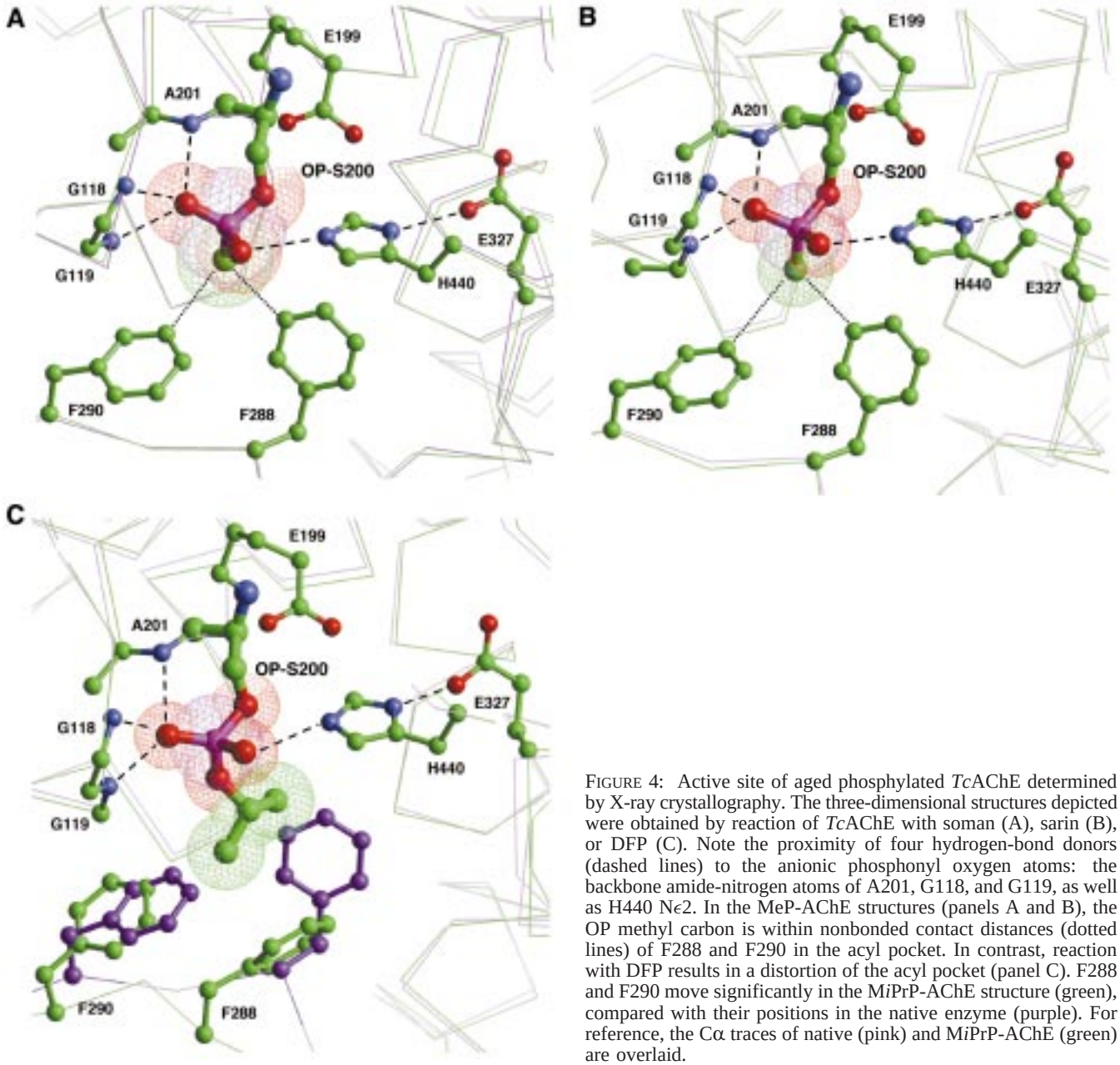

FIGURE 4: Active site of aged phosphylated *Tc*AChE determined by X-ray crystallography. The three-dimensional structures depicted were obtained by reaction of *Tc*AChE with soman (A), sarin (B), or DFP (C). Note the proximity of four hydrogen-bond donors (dashed lines) to the anionic phosphonyl oxygen atoms: the backbone amide-nitrogen atoms of A201, G118, and G119, as well as H440 Nϵ2. In the MeP-AChE structures (panels A and B), the OP methyl carbon is within nonbonded contact distances (dotted lines) of F288 and F290 in the acyl pocket. In contrast, reaction with DFP results in a distortion of the acyl pocket (panel C). F288 and F290 move significantly in the M*i*PrP-AChE structure (green), compared with their positions in the native enzyme (purple). For reference, the Cα traces of native (pink) and M*i*PrP-AChE (green) are overlaid.

oxygen atom (O′ Scheme 2), the bond that breaks during aging is close to the imidazole ring of H440 (Table 3). Furthermore, the departed alkyl group would have filled the solvent-accessible pocket in front of the indole ring of W84 (Figure 3). Dealkylation occurs selectively in this site because the crystal structure shows that DFP lost exclusively the *iso*propyl group in front of W84, while the residual isopropyl group in the acyl pocket is present at full occupancy.

The deduced position of the departed alkyl group in the crystal structures explains several biochemical features of the aging reaction in solution: (1) the catalytic histidine participates in aging (*34*, *39*); (2) dealkylation occurs preferentially in the choline binding subsite (*8*, *40*, *41*), which is now widely accepted to be W84 (*10*, *42*); and (3) aging rate constants for OPs with branched alkyl groups are reduced 60−1100-fold by the site-specific replacement of W86(*84*)[4] in HuAChE (*36*, *43*).

The negative charge introduced by the departure of an alkyl group during aging imposes an important barrier to dephosphylation because anionic phosphoesters are inherently resistant to nucleophilic attack (*44*). Electrostatic repulsion alone, however, does not adequately explain the truly irreversible character of aged enzyme. The presence of a negative charge retards nucleophilic attack of simple phosphorus diesters by only approximately 50−100-fold (*45*), and reactivation of anionic OP-chymotrypsin conjugates by an intramolecular nucleophile is possible (*46*). Furthermore, protein denaturation of aged M*i*PrP-AChE permits significant base-catalyzed dephosphorylation (*47*), suggesting that the resistance of aged OP-AChE to reactivation must be partly caused by specific structural interactions between the folded enzyme and the OP.

Structural Barriers to Enzyme Reactivation. The aged OP-*Tc*AChE structures reveal a remarkable array of possible

[4] The italicized number in parentheses immediately following an amino acid residue is the corresponding residue in the reference structure, *Tc*AChE.

Table 3: Distances between *Tc*AChE Active-site Residues and the OP Moiety

Possible Hydrogen Bonds (Å/deg)[a]

donor···acceptor	MeP-AChE sarin	MeP-AChE soman	M*i*PrP-AChE DFP
H440 Nϵ2···O[b]-P	2.9/154	2.6/173	2.7/168
G118 N···O[c]-P	2.8/165	2.8/160	2.7/161
G119 N···O[c]-P	2.6/152	2.6/161	2.6/158
A201 N···O[c]-P	3.1/ 163	3.0/169	3.0/169

Acyl Pocket Distances (Å)[d]

	sarin	soman	TMTFA complex
F288	4.8	4.8	5.1
F290	4.7	4.8	5.6
G119[e]	4.0	3.9	4.3
W233	4.2	4.3	4.8
F331	5.5	5.5	5.6

[a] Hydrogen bonds were considered possible if the straight-line distance between an appropriate donor and acceptor atom was $\leq$3.5 Å and the angle from donor-hydrogen-acceptor atom was $\geq$120°. For calculation of the angles, the positions of the putative hydrogen atoms were determined from the geometry of the heavy atom positions using INSIGHTII. [b] The residual oxygen atom after dealkylation (depicted as O′ in Scheme 2). [c] The oxygen atom in the oxyanion hole (depicted as O in Scheme 2). [d] Straight-line distance from the methyl carbon atom of the phosphonate, or from the CF_3-carbon atom of TMTFA (*42*), to the geometric center of the phenyl or benzopyrrole ring of the indicated side chain. [e] Straight-line distance to G119 Cα.

noncovalent forces that contribute to the irreversible inhibition which is characteristic of OP nerve agents. Three possible hydrogen bonds from the oxyanion hole (main-chain nitrogen atoms of G118, G119, and A201) to one phosphonyl oxygen atom stabilize the bound OP adduct before and after aging (Table 3). Indeed, this interaction may be strengthened by dealkylation (aging) because electronic rearrangement could place the formal negative charge of the aged OP adduct partly or entirely in the dipolar oxyanion hole. It was shown by site-specific mutagenesis that replacement of the oxyanion hole residues equivalent to either G118 or G119 in HuAChE and HuBChE markedly slows the reaction rate constants for OP inhibitors (*48*−*50*).

The acyl pocket provides another barrier to reactivation. A "dry" hydrophobic patch formed by F288, F290, W233, and G119 Cα completely surrounds one OP alkyl (or alkoxyl) group (Table 3; Figure 2). This could limit dephosphylation by blocking access of attacking water molecules to the correct face of the phosphorus, as well as by providing stabilizing nonbonded contacts to the OP in the case of the sarin or soman (Figure 4). The G119 Cα is only 4.3 Å away from the phosphorus and is almost in-line with the phosphorus-S200 Oγ bond. Placing an imidazole side chain specifically at this position in HuBChE (G117(*119*)H) confers OP hydrolase activity by increasing spontaneous dephosphylation (*49*, *51*).

A key structural feature of aged OP-serine hydrolases appears to be a favorable electrostatic interaction between Nϵ2 of the active-site imidazolium and one oxygen atom of the anionic OP moiety. A hydrogen bond is possible between H440 Nϵ2 (donor) and one oxygen of the OP (acceptor) in each of the three aged OP-*Tc*AChE crystal structures (Table 3). Similar geometry is present in the aged structures of M*i*PrP-trypsin (PDB code 1ntp) (*52*), M*i*PrP-chymotrypsin (1gmh) (*53*), and an MeP-esterase (from *Streptomyces scabies*; 1esd) (*54*). The presence of a hydrogen bond is consistent with the conclusion that the catalytic histidine Nϵ2 is immobilized in a protonated form in the aged enzyme, thereby locking the phosphylated active site in an electrostatic and structural analogue of the natural substrate TI (*55*).

Structural Models for the Deacylation Tetrahedral Intermediate. The active sites of aged MeP-AChE (sarin and soman) provide the best available structural analogues for the negatively charged, *deacylation* TI formed during reaction with the natural substrate, ACh (*55*, *56*). One phosphonyl oxygen in the oxyanion hole mimics the carbonyl oxygen in the substrate TI (*14*), while the other oxgyen atom interacts with the H440 imidazolium. Thus, the anionic OP adduct strongly complements the preformed electrostatic environment of the AChE active site (reviewed in ref *57*). Additionally, the position of the methyl group of sarin and soman should closely approximate that of the ACh methyl group (Scheme 1). Both F288 and F290 provide close nonbonded contacts to the sarin or soman methyl group (Figure 4), supporting the hypothesis that these aromatic side chains also bind the ACh methyl group in the substrate TI (*42*).

The side chain of W233 is proximal to the methyl group in the MeP-AChE structure (deacylation TI analog), as well as to the CF_3 group in the structure of *Tc*AChE inhibited with m-(*N*,*N*,*N*-trimethylammonio)-2,2,2-trifluoroacetophenone (TMTFA; *42*) (acylation TI analog) (Table 3). Furthermore, W233 is absolutely conserved in AChE and BChE, as is the adjacent P232 that constrains the position of the indole ring. The proximity and invariant position of W233 suggest to us a more general and primary role for this acyl pocket residue in catalysis; replacement of W233 in HuBChE was shown recently to result in a 32-fold decrease in the k_{cat} for substrate hydrolysis (*58*).

Movement of the Acyl Pocket in MiPrP-AChE. Structure−activity studies first suggested the presence of specific binding pockets in the active site of cholinesterase that interact with the acyl and alkoxy groups of carboxyl ester substrates and OP inhibitors (reviewed in refs *6*, *59*). This approach showed convincingly that the acyl pocket of AChE was more restrictive than that of BChE. After the crystal structure of *Tc*AChE became available, two aromatic residues, F288 and F290, were implicated as the source of AChE selectivity on the basis of sequence alignments and site-specific mutagenesis data (reviewed in ref *15*).

Movement of F288 and F290 during the reaction with DFP, but not with sarin or soman (Figure 4), supports the idea that the aromatic side chains of these residues are the primary source of acyl pocket selectivity in *Tc*AChE. Previous molecular dynamics studies of *Tc*AChE suggested either that the degrees of freedom available to substrates and inhibitors were restricted by F288 and F290 or that the side chains underwent compensatory movements to accommodate bulky ligands; the models did not predict that the polypeptide backbone atoms in the acyl pocket could move almost 5 Å (Figure 5). Concurrent movement of the phenyl rings of F331, F288, and F290 suggests that a network of cooperative $\pi-\pi$ interactions may stabilize the acyl-binding pocket in native *Tc*AChE.

The free-energy penalty associated with the observed conformational change in the acyl pocket offers a concrete explanation for the substrate specificity of *Tc*AChE. The

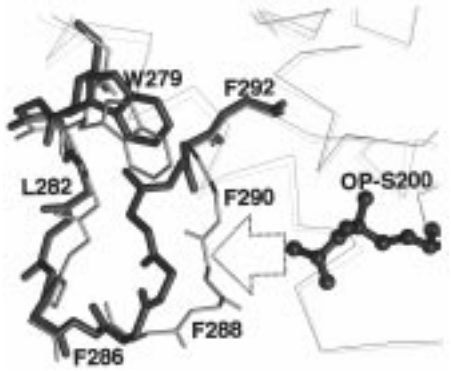

FIGURE 5: Conformational change in the acyl pocket. The main chain of M*i*PrP-AChE (thicker dark sticks) is compared with that of native *Tc*AChE (thinner gray sticks) from position 278 to 292. The main chain displacement in the M*i*PrP-AChE stems from steric clashes between the bulky *iso*propyl group of DFP and the side chains of F288 and F290 (indicated by the arrow and also depicted in Figure 4C). The movement occurs on a loop that includes W279 (side chain shown) of the peripheral site. For reference, the Cα traces (thin lines) of the superimposed proteins are shown.

reversible dissociation constant with DFP, for example, is 2−3 orders of magnitude higher for either *Tc*AChE or HuAChE than it is for HuBChE (Table 1). Replacement of the acyl pocket residues F295(*288*) and F297(*290*) in HuAChE with the smaller aliphatic side chains found in HuBChE abolishes this difference (*17*, *18*). Likewise, the specificity constants for reaction of HuAChE or *Tc*AChE with a substrate containing a butyryl group are 100−450-fold lower than those for reaction with an optimal substrate containing a methyl group (Table 1).

If *Tc*AChE is phosphorylated with DFP and then rapidly dephosphorylated with an oxime nucleophile before aging can occur, the regenerated enzyme is essentially identical with native enzyme in its substrate specificity and affinity for a range of fluorescent bisquaternary ammonium ligands (*38*). Therefore, the conformational change we observe is probably reversible upon reactivation. The aging reaction stops dephosphorylation, however, and traps the acyl pocket of aged M*i*PrP-*Tc*AChE in a conformation that may occur transiently during reaction with some substrates and inhibitors. Because the acyl pocket loop that moves also includes W279, which forms an important part of the AChE peripheral site (reviewed in ref *15*), it is reasonable to speculate that this loop conjoins the active site with the peripheral site during catalysis (Figure 5). Such a link was first proposed by Changeux (*60*) to explain the allosteric binding of certain inhibitors to *Torpedo* AChE, but it continues to elude firm experimental proof.

Despite evidence in the literature for conformational changes associated with aging of some OP-AChE, -BChE, and -chymotrypsin conjugates in solution (*61*−*63*), we detected no major structural rearrangements in *Tc*AChE as a result of the aging reaction itself. It remains possible, however, that reversible conformational changes occurred on the pathway to the final aged OP-*Tc*AChE structures. We are testing this possibility by ongoing X-ray crystallographic studies of nonaged OP-*Tc*AChE complexes.

ACKNOWLEDGMENT

We thank Ms Lilly Toker for valuable technical assistance. Dr. Clarence A. Broomfield provided advice on the role of the oxyanion hole in aging and reactivation. The opinions or assertions contained herein belong to the authors and are not necessarily the official views of the U.S. Army or the U.S. Department of Defense.

REFERENCES

1. Rosenberry, T. L. (1975) *Adv. Enzymol. Relat. Areas Mol. Biol. 43*, 103−218.
2. Froede, H. C., and Wilson, I. B. (1984) *J. Biol. Chem. 259*, 11010−11013.
3. Bernhard, S. A., and Orgel, L. E. (1959) *Science 130*, 625−626.
4. Aldridge, W. N., and Reiner, E. (1972) *Enzyme inhibitors as substrates: Interactions of esterases with esters of organophosphorus and carbamic acids*, North-Holland Publishing, Amsterdam, The Netherlands.
5. Steitz, T. A., Henderson, R., and Blow, D. M. (1969) *J. Mol. Biol. 46*, 337−348.
6. Jarv, J. (1984) *Bioorg. Chem. 12*, 259−278.
7. Kovach, I. (1988) *J. Enzyme Inhib. 2*, 199−208.
8. Berends, F., Posthumus, C. H., Sluys, I. V. D., and Deierkauf, F. A. (1959) *Biochim. Biophys. Acta 34*, 576−578.
9. Michel, H. O., Hackley, J., B. E., Berkowitz, L., List, G., Hackley, E. B., Gillilan, W., and Pankau, M. (1967) *Arch. Biochem. Biophys. 121*, 29−34.
10. Sussman, J. L., Harel, M., Frolow, F., Oefner, C., Goldman, A., Toker, L., and Silman, I. (1991) *Science 253*, 872−879.
11. Barak, D., Ariel, N., Velan, B., and Shafferman, A. (1992) in *Multidisciplinary Approaches to Cholinesterase Functions* (Shafferman, A., and Velan, B., Eds.) pp 195−199, Plenum Press, New York.
12. Harel, M., Sussman, J. L., Krejci, E., Bon, S., Chanal, P., Massoulié, J., and Silman, I. (1992) *Proc. Natl. Acad. Sci. U.S.A. 89*, 10827−10831.
13. Millard, C. B., and Broomfield, C. A. (1992) *Biochem. Biophys. Res. Commun. 189*, 1280−1286.
14. Robertus, J. D., Kraut, J., Alden, R. A., and Birktoft, J. J. (1972) *Biochemistry 11*, 4293−4303.
15. Taylor, P., and Radic, Z. (1994) *Annu. Rev. Pharmacol. Toxicol. 34*, 281−320.
16. Futerman, A. H., Low, M. G., Ackerman, K. E., Sherman, W. R., and Silman, I. (1985) *Biochem. Biophys. Res. Commun. 129*, 312−317.
17. Ordentlich, A., Barak, D., Kronman, C., Flashner, Y., Leitner, M., Segall, Y., Ariel, N., Cohen, S., Velan, B., and Shafferman, A. (1993) *J. Biol. Chem. 268*, 17083−17095.
18. Ordentlich, A., Barak, D., Kronman, C., Ariel, N., Segall, Y., Velan, B., and Shafferman, A. (1996) *J. Biol. Chem. 271*, 11953−11962.
19. Ellman, G. L., Courtney, K. D., Andres, V., Jr., and Featherstone, R. M. (1961) *Biochem. Pharmacol. 7*, 88−95.
20. Main, A. R., and Dauterman, W. C. (1963) *Nature 198*, 551−553.
21. Hope, H. (1988) *Acta Crystallogr., Sect. B 44*, 22−26.
22. Ravelli, R. B. G., Sweet, R. M., Skinner, J. M., Duisenberg, A. J. M., and Kroon, J. (1997) *J. Appl. Crystallogr. 30*, 551−554.
23. Otwinowski, Z. (1993) in *Data Collection and Processing*, Proceedings of the CCP4 Study Weekend 29−30 January 1993 (Sawyer, L., Isaacs, N., and Bailey, S., Eds.) pp 56−62, SERC, Daresbury, U.K.
24. Raves, M. L., Harel, M., Pang, Y. P., Silman, I., Kozikowski, A. P., and Sussman, J. L. (1997) *Nat. Struct. Biol. 4*, 57−63.
25. Brünger, A. T., and Krukowski, A. (1990) *Acta Crystallogr., Sect. A 46*, 585−593.
26. Adams, P. D., Pannu, N. S., Read, R. J., and Brünger, A. T. (1997) *Proc. Natl. Acad. Sci. U.S.A. 94*, 5018−5023.
27. Brünger, A. T., Adams, P. D., Clore, G. M., DeLano, W. L., Gros, P., Grosse-Kunstleve, R. W., Jian, J. S., Kuszewski, J., Nilges, M., Pannu, N. S., Read, R. J., Rice, L. M., Simonson, T., and Warren, G. L. (1998) *Acta Crystallogr., Sect. D 54*, 905−921.
28. Laskowski, R. A., MacArthur, M. W., Moss, D., and Thornton, J. M. (1993) *J. Appl. Crystallogr. 26*, 283−291.

29. Vriend, G. (1990) *J. Mol. Graphics 8*, 52−56.
30. Schaffer, N. K., May, S. C., Jr., and Summerson, W. H. (1954) *J. Biol. Chem. 206*, 201−207.
31. Benschop, H. P., and de Jong, L. P. A. (1988) *Acc. Chem. Res. 21*, 368−374.
32. Barak, R., Ordentlich, A., Barak, D., Fischer, M., Benschop, H. P., de Jong, L. P. A., Segall, Y., Velan, B., and Shafferman, A. (1997) *FEBS Lett. 407*, 347−352.
33. Jones, T. A., Zou, J.-Y., Cowan, S. W., and Kjeldgaard, M. (1991) *Acta Crystallogr., Sect. A 47*, 110−119.
34. Bender, M. L., and Wedler, F. C. (1972) *J. Am. Chem. Soc. 94*, 2101−2109.
35. Kovach, I. M., Huber, J. H. A., and Schowen, R. L. (1988) *J. Am. Chem. Soc. 110*, 590−593.
36. Shafferman, A., Ordentlich, A., Barak, D., Stein, D., Ariel, N., and Velan, B. (1996) *Biochem. J. 318*, 833−840.
37. Viragh, C., Akhmetshin, R., Kovach, I. M., and Broomfield, C. A. (1997) *Biochemistry 36*, 8243−8252.
38. Taylor, P., and Jacobs, N. M. (1974) *Mol. Pharmacol. 10*, 93−107.
39. Beauregard, G., Lum, J., and Roufogalis, B. D. (1981) *Biochem. Pharmacol. 30*, 2915−2920.
40. Berry, W. K., and Davies, D. R. (1966) *Biochem. J. 100*, 572−576.
41. Boskovic, B., Maksimovic, M., and Minic, D. (1968) *Biochem. Pharmacol. 17*, 1738−1741.
42. Harel, M., Quinn, D. M., Nair, H. K., Silman, I., and Sussman, J. L. (1996) *J. Am. Chem. Soc. 118*, 2340−2346.
43. Barak, D., Ordentlich, A., Segall, Y., Velan, B., Benschop, H. P., de Jong, L. P. A., and Shafferman, A. (1997) *J. Am. Chem. Soc. 119*, 3157−3158.
44. Westheimer, F. H. (1987) *Science 235*, 1173−1178.
45. Kirby, A. J., and Younas, M. (1970) *J. Chem. Soc. B*, 1165−1172.
46. Kaiser, E. T., and Lee, T. W. S. (1971) *J. Am. Chem. Soc. 93*, 2351−2353.
47. Segall, Y., Waysbort, D., Barak, D., Ariel, N., Doctor, B. P., Grunwald, J., and Ashani, Y. (1993) *Biochemistry 32*, 13441−13450.
48. Broomfield, C. A., Millard, C. B., Lockridge, O., and Caviston, T. L. (1995) in *Enzymes of the Cholinesterase Family* (Quinn, D. M., Balasubramanian, A. S., Doctor, B. P., and Taylor, P., Eds.) pp 169−175, Plenum Press, New York.
49. Millard, C. B., Lockridge, O., and Broomfield, C. A. (1995) *Biochemistry 34*, 15925−15933.
50. Ordentlich, A., Barak, D., Kronman, D., Ariel, N., Segall, Y., Velan, B., and Shafferman, A. (1998) *J. Biol. Chem. 273*, 19509−19517.
51. Millard, C. B., Lockridge, O., and Broomfield, C. A. (1998) *Biochemistry 37*, 237−247.
52. Kossiakoff, A. A., and Spencer, S. A. (1981) *Biochemistry 20*, 6462−6474.
53. Harel, M., Su, C. T., Frolow, F., Ashani, Y., Silman, I., and Sussman, J. L. (1991) *J. Mol. Biol. 221*, 909−918.
54. Wei, Y., Schottel, J. L., Derewenda, U., Swenson, L., Patkar, S., and Derewenda, Z. S. (1995) *Nat. Struct. Biol. 2*, 218−223.
55. Kossiakoff, A. A., and Spencer, S. A. (1980) *Nature 288*, 414−416.
56. Ashani, Y., and Green, B. S. (1981) in *Chemical Approaches to Understanding Enzyme Catalysis: Biomimetic Chemistry and Transition State Analogues* (Green, B. S., Ashani, Y., and Chipman, D., Eds.) pp 169−188, Elsevier, Amsterdam, The Netherlands.
57. Warshel, A., Naray-Szabo, G., Sussman, F., and Hwang, J. K. (1989) *Biochemistry 28*, 3629−3637.
58. Masson, P., Legrand, P., Bartels, C. F., Froment, M.-T., Schopfer, L. M., and Lockridge, O. (1997) *Biochemistry 36*, 2266−2277.
59. Kabachnik, M. I., Brestkin, A. P., Godovikov, N. N., Michelson, M. J., Rozengart, E. V., and Rozengart, V. I. (1970) *Pharmacol. Rev. 22*, 355−388.
60. Changeux, J.-P. (1966) *Mol. Pharmacol. 2*, 369−392.
61. Amitai, G., Ashani, Y., Gafni, A., and Silman, I. (1982) *Biochemistry 21*, 2060−2069.
62. Aslanian, D., Grof, P., Renault, F., and Masson, P. (1995) *Biochim. Biophys. Acta 1249*, 37−44.
63. Steinberg, N., van der Drift, A. C. M., Grunwald, J., Segall, Y., Shirin, E., Haas, E., Ashani, Y., and Silman, I. (1989) *Biochemistry 28*, 1248−1253.

BI982678L